A Closed-Loop Multi-Scale Model for Intrinsic Frequency-Dependent Regulation of Axonal Growth

Fan Bai[a], Richard Bertram[a,b,c], and Bhargav R. Karamched [*a,b]

[a]Deparment of Mathematics, Florida State University, Tallahassee FL 32306, United States
[b]Program in Molecular Biophysics, Florida State University, Tallahassee FL 32306, United States
[c]Program in Neuroscience, Florida State University, Tallahassee FL 32306, United States

Highlights

- A multi-scale closed loop model for axonal length regulation, incorporating motor-motor interactions and including a back end signaling pathway, is developed
- This model captures two key experimental findings
- The model predicts that increasing motor density will cause an axon to grow, thereby providing key insight into what future experiments need to be done to validate the model and understand axonal length control.

Abstract

This article develops a closed-loop multi-scale model for axon length regulation based on a frequency-dependent negative feedback mechanism. It builds on earlier models by linking molecular motor dynamics to signaling delays that then determine signal oscillation period. The signal oscillation is treated as a front end for a signaling pathway that modulates axonal length. This model is used to demonstrate the feasibility of such a mechanism and is tested against two previously published reports in which experimental manipulations were performed that resulted in axon growth. The model captures these observations and yields an expression for equilibrium axonal length. One major prediction of the model is that increasing motor density in the body of an axon results in axonal growth—this idea has not yet been explored experimentally.

Key Words: delayed feedback, TASEP, signaling pathway, length regulation, bifurcation.

1 Introduction

An axon is a long protrusion from the cell body of a neuron whose length can be hundreds or thousands of times larger than the diameter of the cell body. It transmits electrical impulses from the cell body to downstream target neurons. In the first stage of the development of an axon, a growth cone forms and leads its spontaneous extension. In the second stage, the axon tip approaches its targets and synapses ultimately form [1, 2]. The growth rate during this second stage depends on factors released by the target cells [3, 4]. What determines the growth rate during the first stage? This question is the focus of this study.

An axon is composed of microtubules in its center, membrane wrapping the microtubules, and cytosol between the microtubles and the membrane (Fig. 1). Microtubules are directionally polarized filaments with biophysically distinguishable "+" ends and "–" ends [5]. They provide structural integrity for cells and form filaments upon which molecular motors move to transport various cargo such as proteins that can act as signaling molecules [6–8]. The polarity at a given end of the microtubule dictates what kind of molecular motor will travel along in a given direction. For example, kinesins generally walk in the "+" direction along microtubules whereas dyneins tend to walk in the "–" direction. Motor dynamics along microtubules has been the focus of many theoretical investigations in recent years [9–12].

Recently, Rishal et al. proposed a possible mechanism for axon length regulation [13–15] based on bidirectional motor transport (Fig. 1). They hypothesized that an excitatory signal E was carried by kinesins from the cell body to the axon tip, where it induced an inhibitory signal I. This signal was assumed to be transported by dyneins from the tip to the cell body and suppress the signal E. With sufficient time delays, oscillations in both signals arise, which they proposed was the key to axon length sensing . In particular, information regarding axonal length could be encoded in the oscillation frequency, which could be used to regulate axon growth. Encoding information with oscillatory signals has been shown to be advantageous over constant signals in some biological systems [16, 17].

*Corresponding author at: Department of Mathematics, Florida State University, Tallahassee, FL 32306, United States. E-mail address: bkaramched@fsu.edu (Bhargav R. Karamched).

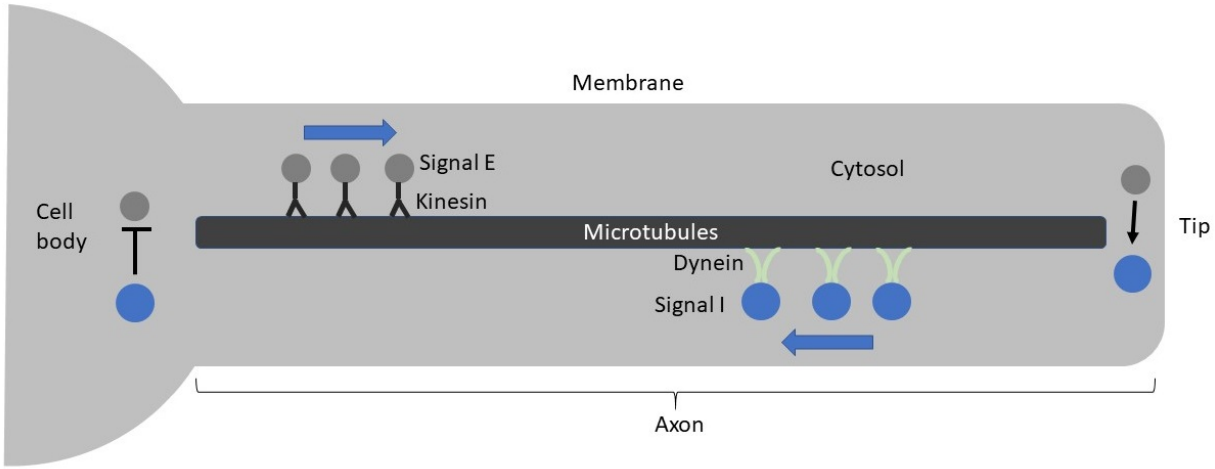

Figure 1: A schematic diagram showing the structure of an axon and the delayed-feedback mechanism proposed by Rishal et al. [13]. The axon is composed of microtubules, cytosol and membrane. The molecular motors, kinesins and dyneins, move along the microtubules in opposite directions and carry the excitatory signal E and inhibitory signal I, respectively. After arriving at the axon tip, the signal E promotes the production of the signal I, which suppresses the production of the signal E when it reaches the cell body.

Based on this hypothesis, Karamched et al. developed a delayed feedback model that was used to show that oscillations appeared when the axon length crossed some threshold (a supercritical Hopf bifurcation point) and demonstrated a negative correlation between the frequency and the length [18]. The model also replicated the experimental result that knockdown of either kinesin or dynein caused axon growth [13]. A follow-up study by Folz et al. added downstream signaling pathways to the model of Karamched et al. that provided a possible mechanism by which a neuron could decode the length information in the oscillating signals [19]. In spite of the progress in modeling, several aspects of this frequency-dependent length regulation remain unclear. First, neither model includes the possible influence of motor-motor interactions upon motor densities in the axon and thus on the delays. Second, a follow-up experimental study by Perry et al. showed that importin-β_1 mRNA and its protein product (importin β_1) could serve as the excitatory and inhibitory signal, respectively [20]. Disrupting the interaction between the mRNA and its carriers (kinesins) was shown to induce axon growth. This is a key test of the axon growth mechanism, and it is not clear whether this can be explained by the frequency-dependent mechanism.

In this article, we begin with the model of Karamched et al. and build on it by explicitly considering the transport of E and I signals by kinesin and dynein motors and by considering interactions between motors. This allows us to determine the relationship between axon length and the time delays that is key to the oscillation mechanism. We then form a closed-loop system that allows us to simulate experimental manipulations performed in [13, 20]. The closed-loop model also facilitates an analysis of how the equilibrium axon length varies with system parameters, and we demonstrate step-like changes that can be linked to the initiation/termination of oscillations in the E-I system.

2 How are oscillations in signaling molecules generated?

The basis for axon length detection in the mechanism postulated in [13] relies on oscillations in the concentration of signaling molecules. It is postulated that these oscillations are the result of delayed negative feedback of an inhibitory signaling molecule I on an excitatory signaling molecule E. To demonstrate this mathematically, we use a system of delay differential equations that describe the processes in Fig. 1. Let E_b, I_b and E_t, I_t be the concentrations of E and I in the cell body and axon tip, respectively. Their temporal evolution is described by the following:

$$\frac{\mathrm{d}E_b}{\mathrm{d}t} = p_{E,b}(t) - d_{E,b}E_b(t) - w_E J_K E_b(t), \tag{1}$$

$$\frac{\mathrm{d}E_t}{\mathrm{d}t} = -d_{E,t}E_t(t) + r_V w_E J_K E_b(t-\tau_K), \tag{2}$$

$$\frac{\mathrm{d}I_b}{\mathrm{d}t} = -d_{I,b}I_b(t) + w_I J_D I_t(t-\tau_D)/r_V, \tag{3}$$

$$\frac{\mathrm{d}I_t}{\mathrm{d}t} = p_{I,t}(t) - d_{I,t}I_t(t) - w_I J_D I_t(t), \tag{4}$$

where $p_{E,b}$ and $p_{I,t}$ are the production rates of E and I. A Hill function H describes the activation of I by E:

$$p_{I,t} = p_I H\left(E_t, K_I, n_I\right), \tag{5}$$

where

$$H\left(x, K, n\right) = \frac{x^n}{x^n + K^n}. \tag{6}$$

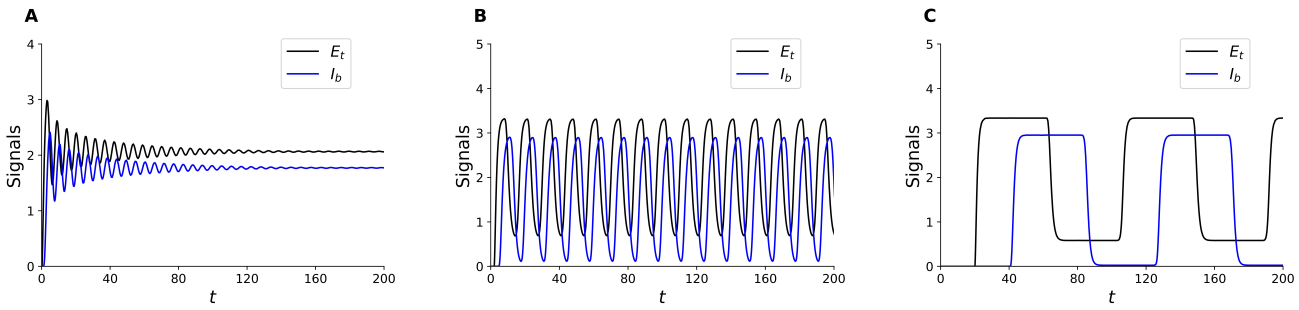

Figure 2: Solutions of the delayed feedback model for different delay values. (A) $\tau_K = \tau_D = 0.2$. (B) $\tau_K = \tau_D = 2$. (C) $\tau_K = \tau_D = 20$. Other parameter values are given in Table 1.

In Eq. (5), p_I is the maximum production rate, K_I is the half-activation level, and n_I is the Hill coefficient for the signal I. A Hill function also describes the suppression of E by I:

$$p_{E,b} = p_E(1 - H(I_b, K_E, n_E)), \tag{7}$$

where p_E is the unsuppressed production rate and the parameters K_E and n_E are analogous to K_I and n_I. The term $w_E J_K E_b(t)$ in Eq. (1) reflects the transport of E away from the cell body by kinesin motors. The quantity J_K is the current of the kinesin motors through the axon; it is the number of kinesin motors entering the axon or arriving at the axon tip per unit time. The quantity w_E represents the average number of E molecules carried by a single kinesin and reflects the binding affinity of E to kinesin motors. The delay τ_K in Eq. (2) represents the average time for a kinesin motor to traverse the distance from the cell body to the axon tip, so the term $r_V w_E J_K E_b(t - \tau_K)$ corresponds to the arrival of the signal E at the tip. This term includes the volume fraction, r_V, of the axon body to the axon tip. Similarly, $w_I J_D I_t(t)$ and $w_I J_D I_t(t - \tau_D)/r_V$ in Eqs. (4) and (3) describe retrograde transport of I by dynein motors. The terms $d_{E,b}E_b$, $d_{E,t}E_t$, $d_{I,b}I_b$ and $d_{I,t}I_t$ describe natural degradation of E and I.

The current model improves on an earlier one [18] by explicitly describing the dependence of the production of each signal on the concentration of the other signal (Eqs. (5) and (7)). It is motivated by the experimental finding that importin-β_1 mRNA may act as the signal E, whose product (importin-β_1 protein) may act as the signal I [20]. The translation of importin-β_1 occurs at the axon tip, thereby spatially separating the mRNA production from the protein production. It is not yet clear how importin-β_1 protein inhibits the production of importin-β_1 mRNA, but it is likely through repression of gene transcription. Our model does not specify the identity of the signaling molecules, or the means of production. Rather, it is more general, relying only on the spatial segregation of the E and I production sites and the mutual feedback between the two.

We use a dimensionless form of Eqs. (1)–(4), as shown in the next section. They are very similar, except that the volume ratio r_V scales out. To investigate the effects of changes in the time delays on system dynamics, the dimensionless equations, Eqs. (20)–(23), are solved numerically by using the "dde23" solver in MATLAB [21]. The initial conditions are $E_b(t) = E_t(t)$ for $t \in [-\tau_K, 0]$ and $I_b(t) = I_t(t) = 0$ for $t \in [-\tau_D, 0]$. The values of the delays are given in the caption of Fig. 2, and other parameter values are given in Table 1. For small time delays, numerical calculation shows that there is a stable equilibrium following transient oscillations (Fig. 2A). As the delays are increased, the stable equilibrium bifurcates into a limit cycle as the system undergoes a supercritical Hopf bifurcation. The oscillations are nearly sinusoidal for delays close to the critical values for oscillation initiation (Fig. 2B) and approach a square wave form as the delays are increased further (Fig. 2C). In the latter case, each signal remains at its maximal or minimal value for a duration of approximately $\tau_K + \tau_D$ time units, with very rapid switches between (Fig. 2C). This is shown in more detail in Fig. 3, which includes all four state variables. It can be seen that E_b starts to grow rapidly around $t = 850$ (black curve). After time τ_K time units, the signal E reaches the axon tip, leading to a rapid increase in E_t (blue curve). This causes the production of the signal I at the tip, corresponding to the increase in I_t (green curve). The signal I then travels retrogradely and reaches the cell body after τ_D. This leads to a quick increase in I_b (red curve) and a decrease in E_b (black curve). The axon tip senses the low level of E_b after τ_K and stops producing the signal I, resulting in a drop in I_t. This drop leads to a drop in I at the cell body after τ_D time units, allowing E_b to rise again and starting a new cycle. Therefore, the oscillation period T is

$$T \approx 2(\tau_K + \tau_D). \tag{8}$$

3 What is the relationship between the oscillation period and the axon length?

To relate the signal oscillation period with axonal length, we next model the transportation of the signals along an axon by molecular motors as a Totally Asymmetric Simple Exclusion Process (TASEP) [22–25], which is illustrated in Fig. 4. This enables us to relate the delays to the axon length. Furthermore, the TASEP provides relations between the

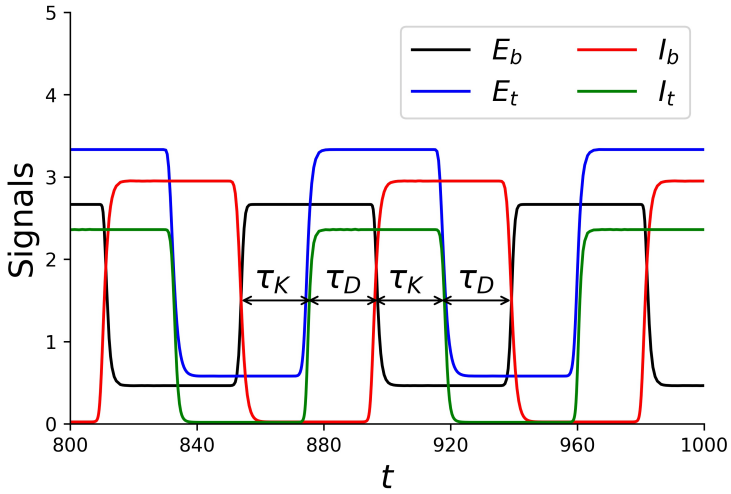

Figure 3: Square-wave oscillations that occur when $\tau_K = \tau_D = 20$. The oscillation period is approximately $2(\tau_K + \tau_D)$.

motor currents (J_K and J_D) and the motor densities. These relations are combined with the delayed feedback model to describe how the oscillation period varies with various biophysical parameters—specifically bulk motor density and motor-signal affinity.

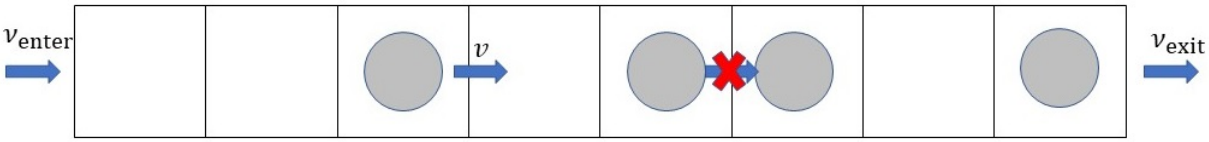

Figure 4: The Totally Asymmetric Simple Exclusion Process (TASEP). In this process, particles enter a lane of lattice sites with rate ν_{enter} and exit with rate ν_{exit}. After entry, each particle hops to its next site with rate ν, provided the site is empty.

Multiple microtubule tracks traverse the axon. The molecular motors kinesin and dynein traverse these tracks with periods of ballistic motion interspersed with periods of track switching [26]. However, it has been shown that the motor transport along multiple tracks is mathematically equivalent to motor transport along a single track, in an average sense [27]. We therefore model the motion of kinesin along a single track and dynein along a second track. The kinesin and dynein dynamics are each described with a TASEP that consists of a lane of lattice sites and multiple particles that move along the lane (see Fig. 5). Specifically, a particle at some site can only jump to the next site if the latter is unoccupied. The probability for such a successful jump within a small time duration $\mathrm{d}t$ is $\nu \mathrm{d}t$, where ν is the hopping rate constant. Particles enter the lane through the first site and leave from the last, and the corresponding rate constants are ν_{enter} and ν_{exit}. We assume $\nu_{\text{enter}} = \nu_{\text{exit}} = \nu$.

To derive a relation between τ_K and the TASEP parameters, we invoke a mean-field approximation [28]. Let N be the total number of sites of the lane for the kinesin motors and ν_K be the hopping rate (we assume that it is the same with or without cargo). The state of site i can be described by an occupation number $O_{K,i}(t)$, defined as

$$O_{K,i}(t) = \begin{cases} 0 & \text{site } i \text{ is vacant,} \\ 1 & \text{site } i \text{ is occupied.} \end{cases} \tag{9}$$

With time discretized into units of $\mathrm{d}t$, the conditional probability for a kinesin to jump to site $i+1$ at $t_0 + \mathrm{d}t$, provided it is at site i at t_0, is given by

$$\Pr\{\text{at site } i+1 \text{ at } t_0 + \mathrm{d}t | \text{at site } i \text{ at } t_0\} = (1 - O_{K,i+1}(t_0))\nu_K \mathrm{d}t. \tag{10}$$

Then the conditional probability for the kinesin to jump to site $i+1$ at $t_0 + 2\mathrm{d}t$, provided that it is at site i at t_0, is

$$\begin{aligned} &\Pr\{\text{at site } i+1 \text{ at } t_0 + 2\mathrm{d}t | \text{at site } i \text{ at } t_0\} \\ &= \Pr\{\text{at site } i+1 \text{ at } t_0 + 2\mathrm{d}t | \text{at site } i \text{ at } t_0 + \mathrm{d}t\} \cdot \Pr\{\text{at site } i \text{ at } t_0 + \mathrm{d}t | \text{at site } i \text{ at } t_0\} \\ &= (1 - O_{K,i+1}(t_0 + \mathrm{d}t))\nu_K \mathrm{d}t[1 - (1 - O_{K,i+1}(t_0))\nu_K \mathrm{d}t]. \end{aligned} \tag{11}$$

Continuing this process, the conditional probability for the kinesin to jump to site $i+1$ at $t_0 + n\mathrm{d}t$, provided that it

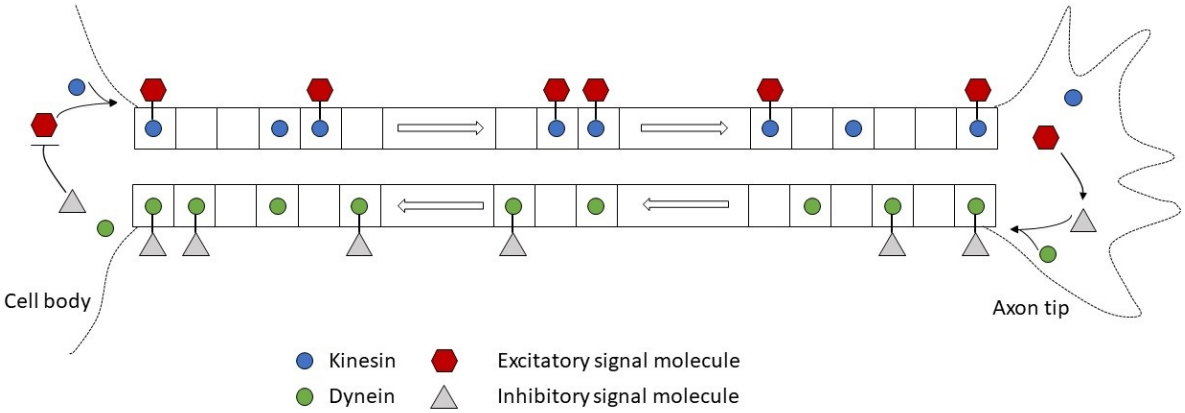

Figure 5: Bidirectional transport of signaling molecules along an axon is the basis of the delayed feedback model. Excitatory signaling molecules E (red hexagons) are produced in the cell body and transported by kinesins (blue circles) to the axon tip, where they promote the production of inhibitory signaling molecules I (grey triangles). These molecules are carried by dyneins (green circles) to the cell body where they suppress the production of the signal E. The degradation of the E and I molecules is not shown. The microtubules along which the motors travel are modeled as two lanes of lattice sites.

is at site i at t_0, is

$$\begin{aligned}&\Pr\{\text{at site } i+1 \text{ at } t_0+n\mathrm{d}t|\text{at site } i \text{ at } t_0\}\\&=(1-O_{K,i+1}(t_0+(n-1)\mathrm{d}t))\nu_K\mathrm{d}t\prod_{i=1}^{n-1}[1-(1-O_{K,i+1}(t_0+(i-1)\mathrm{d}t))\nu_K\mathrm{d}t].\end{aligned}\tag{12}$$

Let $\rho_{K,i}$ be the ensemble average of $O_{K,i}(t)$ at equilibrium. By the mean-field approximation [28], the probability for a kinesin motor to stay at site i for ndt time units can be calculated by replacing all the occupation numbers at different times by their ensemble average $\rho_{K,i+1}$, namely

$$\Pr\{\text{Stay for } n\mathrm{d}t\}=(1-\rho_{K,i+1})\nu_K\mathrm{d}t(1-(1-\rho_{K,i+1})\nu_K\mathrm{d}t)^{n-1},\tag{13}$$

We also set $t_0=0$ since the TASEP is autonomous. The average duration r_i that a kinesin stays at site i is then given by

$$\begin{aligned}r_i&\equiv\sum_{n=1}^{\infty}n\mathrm{d}t(1-\rho_{K,i+1})\nu_K\mathrm{d}t(1-(1-\rho_{K,i+1})\nu_K\mathrm{d}t)^{n-1}\\&=\frac{1}{\nu_K(1-\rho_{K,i+1})},\end{aligned}\tag{14}$$

where the second equality is proved in Appendix A.

It has been shown that $\rho_{K,i}$ is nearly uniform for most bulk sites in the lane [29–31]. There can be boundary layers at either the entrance or the exit or both, but we ignore their contribution to the total residence time of a kinesin within the lane, i.e., the delay τ_K, because the boundary layers encompass only a small number of sites. Let $\rho_{K,\mathrm{bulk}}$ be the constant for the bulk sites, then using this approximation, the total time required for a kinesin molecule to move from the axon body to its tip is

$$\tau_K=\sum_{i=1}^{N}r_i=\frac{N}{\nu_K(1-\rho_{K,\mathrm{bulk}})}.\tag{15}$$

Let L be the axon length and a the size of a single lattice site, then $N=L/a$ and Eq. (15) becomes

$$\tau_K=\frac{L}{a\nu_K(1-\rho_{K,\mathrm{bulk}})}.\tag{16}$$

Thus, τ_K is proportional to L, which coincides with previous models [18, 19]. However, it also indicates that τ_K becomes large if the motors crowd the lane (i.e., if $\rho_{K,\mathrm{bulk}}\approx 1$), which was not considered in previous models. From an identical derivation,

$$\tau_D=\frac{L}{a\nu_D(1-\rho_{D,\mathrm{bulk}})},\tag{17}$$

where ν_D is the hopping rate of the dynein motors and $\rho_{D,\mathrm{bulk}}$ is the average of the occupation numbers for the bulk sites in steady state. We refer to $\rho_{K,\mathrm{bulk}}$ and $\rho_{D,\mathrm{bulk}}$ as the bulk densities of kinesin and dynein motors, respectively.

Parameter	Definition	Value
p_E	Basal production rate of signal E molecules at the cell body	6
p_I	Basal production rate of signal I molecules at the cell body	6
w_E	Average number of signal E molecules carried by a single kinesin	5
w_I	Average number of signal I molecules carried by a single dynein	5
ν_K	Hopping rate of kinesins	1
ν_D	Hopping rate of dyneins	1
$\rho_{K,\text{bulk}}$	Bulk density of kinesins	0.5
$\rho_{D,\text{bulk}}$	Bulk density of dyneins	0.5
$d_{E,b}$	Degradation rate of signal E molecules at the cell body	1
$d_{E,t}$	Degradation rate of signal E molecules at the axon tip	1
$d_{I,b}$	Degradation rate of signal I molecules at the cell body	1
$d_{I,t}$	Degradation rate of signal I molecules at the axon tip	1
L	Axon length	10

Table 1: Dimensionless parameter descriptions and values. Values of p_E, p_I, w_E, w_I, $d_{E,b}$, $d_{E,t}$, $d_{I,b}$ and $d_{I,t}$ are adopted from the previous model [18]. For simplicity, we assume that the hopping rates of kinesins and dyneins are the same (for a discussion on different hopping rates, please see Section 7). By choosing the characteristic hopping rate (v^* in the appendix) to be the rate for kinesins, we get $\nu_K = \nu_D = 1$. We choose $\rho_{K,\text{bulk}} = \rho_{D,\text{bulk}} = 0.5$ in order to get maximum currents (see Eq. (25)). The value of L is set to be 10, such that the signals oscillate like square waves.

Like τ_K, the current J_K of the kinesin motors also depends on $\rho_{K,\text{bulk}}$ [27, 29–31], whose mean field approximation to leading order in a is [23]

$$J_K = \nu_K \rho_{K,\text{bulk}}(1 - \rho_{K,\text{bulk}}). \tag{18}$$

This relation indicates that J_K is symmetric about its maximum value, which occurs at $\rho_{K,\text{bulk}} = 0.5$. The decline in J_K after $\rho_{K,\text{bulk}}$ passes 0.5 reflects crowding of the motors. The approximation for J_D is the same:

$$J_D = \nu_D \rho_{D,\text{bulk}}(1 - \rho_{D,\text{bulk}}). \tag{19}$$

The times required for motors to move from one end of the axon to the other, τ_K and τ_D, become time delays for the signaling molecule concentrations. With the above relations for the delays and currents, a dimensionless system of delay differential equations, with characteristic scales detailed in Appendix 2, is:

$$\frac{\mathrm{d}E_b(t)}{\mathrm{d}t} = p_{E,b}(t) - d_{E,b}E_b(t) - w_E J_K E_b(t), \tag{20}$$

$$\frac{\mathrm{d}E_t(t)}{\mathrm{d}t} = -d_{E,t}E_t(t) + w_E J_K E_b(t - \tau_K), \tag{21}$$

$$\frac{\mathrm{d}I_b(t)}{\mathrm{d}t} = -d_{I,b}I_b(t) + w_I J_D I_t(t - \tau_D), \tag{22}$$

$$\frac{\mathrm{d}I_t(t)}{\mathrm{d}t} = p_{I,t}(t) - d_{I,t}I_t(t) - w_I J_D I_t(t), \tag{23}$$

and the expressions for the dimensionless delays and currents are

$$\tau_K = \frac{L}{\nu_K(1 - \rho_{K,\text{bulk}})}, \quad \tau_D = \frac{L}{\nu_D(1 - \rho_{D,\text{bulk}})} \tag{24}$$

$$J_K = \nu_K \rho_{K,\text{bulk}}(1 - \rho_{K,\text{bulk}}), \quad J_D = \nu_D \rho_{D,\text{bulk}}(1 - \rho_{D,\text{bulk}}). \tag{25}$$

For simplicity, we use the same notation for the dimensionless equations as for the previous dimensional equations. For the remainder of the study we use the dimensionless variables and equations. Parameter values are given in Table 1 unless used as a bifurcation parameter.

From Eqs. (16) and (17), the axon length L affects the time delays linearly. The diagrams in Fig. 6 show how changes in L influence oscillations in I_b (and thereby E_b). At a small value of L, the equilibrium solution (black) loses stability (Fig. 6A), and gives rise to a branch of periodic solutions (red). These solutions are depicted with two curves, one for the oscillation minimum and one for the maximum. After the emergence of the periodic branch at a supercritical Hopf bifurcation (green filled circle) the oscillation amplitude (distance between the red curves) grows quickly and after $L = 1$ changes very little. In contrast, the oscillation period, shown in Fig. 6B, grows almost linearly over the entire range of L values shown. Thus, oscillation period, but not amplitude, is capable of encoding axonal length.

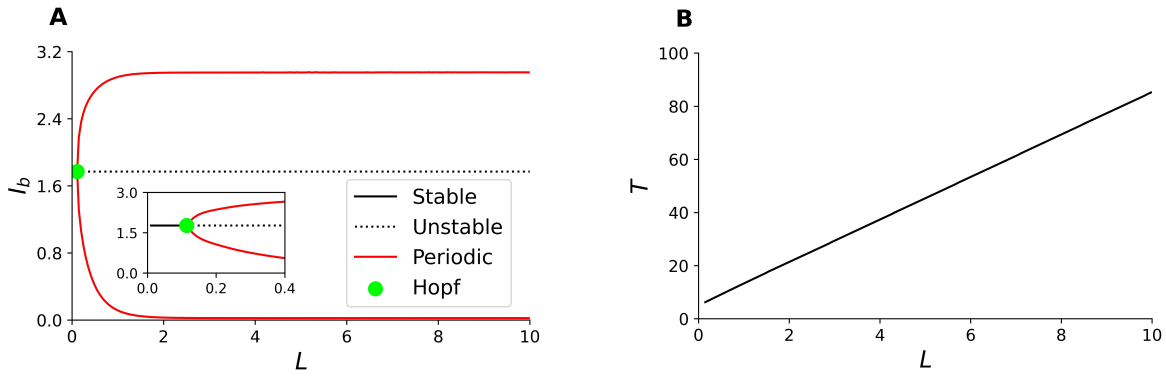

Figure 6: The bifurcation diagram and period variation with respect to L. (A) The bifurcation diagram shows that an oscillatory solution emerges from a supercritical Hopf bifurcation point (green circle) and the oscillation maximum and minimum (red curves) rapidly flatten out as L increases. The stationary branch is generated numerically using the BIFTOOL software package [32], and the periodic branch is generated through numerical integration of the equations over a range of L values. (B) The period T increases almost linearly with L.

4 Experimental manipulations support an inhibitory role for oscillations

If our assumption that axon growth is determined by the oscillation period of the signaling molecules E and I is correct, then since the period increases with axon length in our model, it must be true that axon growth is inhibited at larger periods. Otherwise, the axon would grow without bound. Also, we assume that the axon grows when the signal is at a low level equilibrium, because there is no inhibitory influence to act against the growth. In this section, we explore two experimental manipulations that have been performed which, together with bifurcation analysis, support these features of the model.

In one manipulation, Perry et al. used the anti-nucloelin aptamer AS1411 to disrupt the binding between kinesins and nucleolins and found that it led to axon growth [20]. The nucleolins carry importin-β_1 RNA, which was assumed to be the excitatory signaling molecule E. Thus, application of AS1411 would result in a reduction in w_E, since this parameter reflects the binding affinity between signal E and kinesins. To investigate the effect of application of AS1411 in the model, we performed a bifurcation analysis of the E-I system with respect to w_E (Fig. 7). For a large range of values of w_E there is little change in either the amplitude or period of oscillations. However, for values of w_E below the Hopf bifurcation, the oscillations are replaced by a branch of stable stationary solutions. Since the signaling system is not oscillating here, there is no inhibition of axon growth, so for w_E values below the Hopf bifurcation the axon would grow. Thus, we interpret the experimental manipulation as reducing w_E from a value in which oscillations occur and provide an inhibitory influence to further axon growth, to a value in which there are no oscillations to inhibit axon growth, so the axon increases in length, as observed in the experiments.

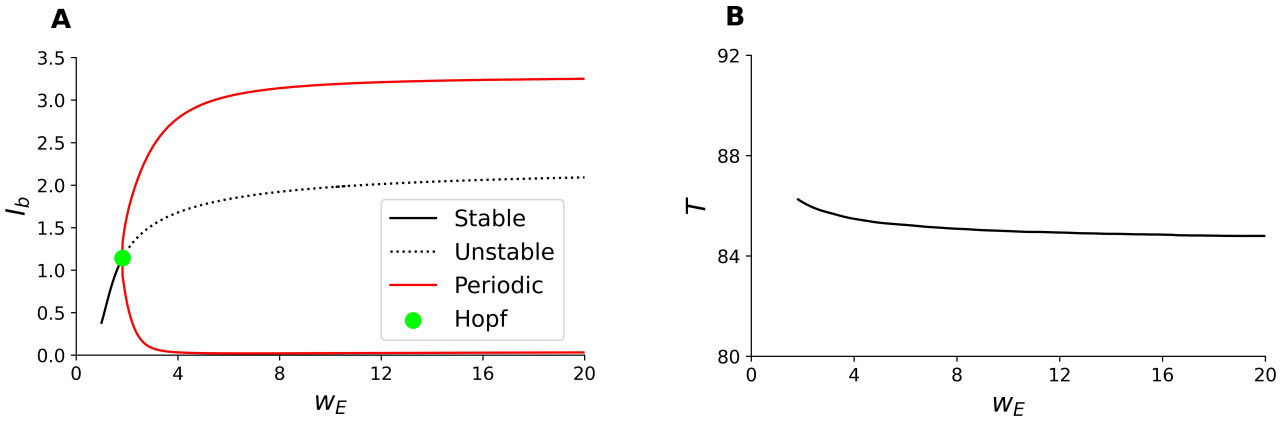

Figure 7: Analysis of signaling molecule oscillations with changes in the binding affinity between E and kinesins (w_E). (A) The one-parameter bifurcation diagram shows that the oscillation starts at a Hopf bifurcation point of w_E (green circle) and the peak value rapidly flattens out. (B) There is little change in period with w_E.

In another manipulation, Rishal et al. reduced the motor densities by knocking down the related motor heavy chains, and in response observed axon growth [13]. To check consistency with our model, we performed bifurcation analysis with respect to the average bulk densities $\rho_{K,\text{bulk}}$ and $\rho_{D,\text{bulk}}$. In both cases, oscillations occur at intermediate levels of the densities, and these are deliminated by Hopf bifurcations. Also, in both cases, the oscillation period increases monotonically with the bulk density (Fig. 8B, D). Thus, a manipulation that reduces the bulk density of

either type of motor would reduce the oscillation period. This reduction would promote axon growth, as seen in the experiments.

Considering both experiments and the corresponding bifurcation analysis, we conclude that the overall effect of the oscillation on axon growth is inhibitory, and the inhibition is stronger at greater periods. In the next section, we implement this by combining the delayed feedback model with a generic signaling pathway for axon growth.

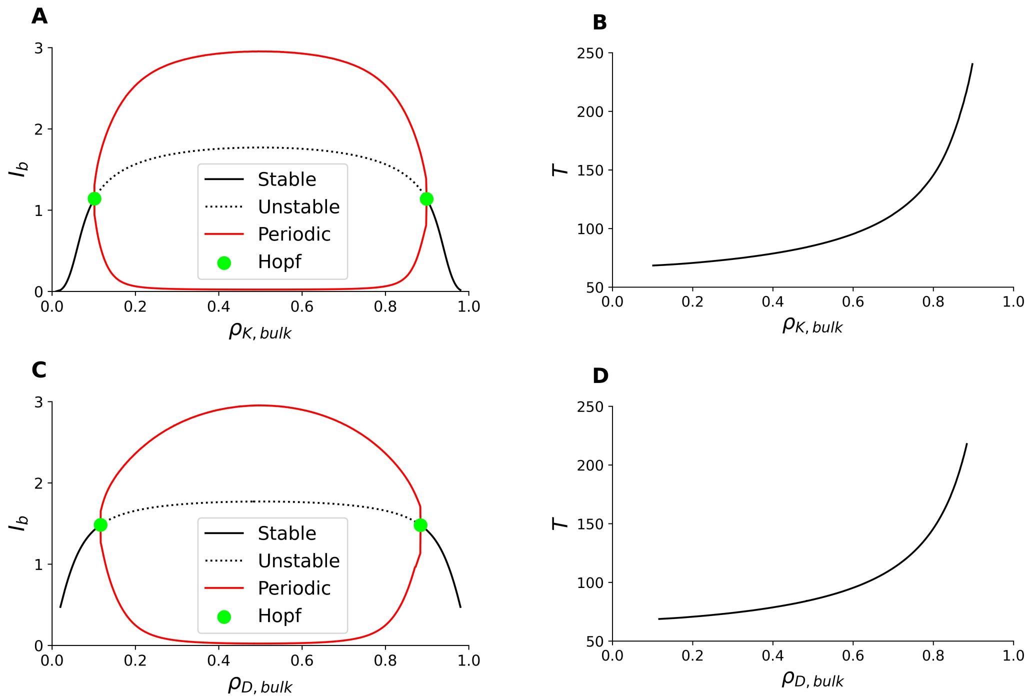

Figure 8: Analysis of signaling molecule oscillations with changes in the bulk densities ($\rho_{K,\text{bulk}}$ and $\rho_{D,\text{bulk}}$). (A, C) The bifurcation diagrams show that oscillations are initiated and terminated by supercritical Hopf bifurcations. (B, D) The period increases with increases in the bulk densities.

5 How does a neuron regulate the length of its axon according to the signal frequency?

Most materials for axon growth are produced in the cell body and transported into an axon [33, 34], although there are also organelles within the axon that enable local production [15, 35]. To regulate axonal growth according to the oscillatory signals, there must be signaling pathways that link the signals to some effector proteins which control the production of the materials in the cell body. In this section, we analyze the following minimal signaling pathway

$$I_b \longrightarrow\!\!\!\!| \; Y \longrightarrow X, \tag{26}$$

which provides a phenomenological description of a mechanism that could be used by a neuron to regulate its axon length. The concentration of the inhibitory signal I at the cell body, I_b, is chosen to be the input in this pathway, which inhibits an intermediate signaling protein Y. Y subsequently activates an effector protein X, which is assumed to positively regulate the production of materials for axon growth in the cell body. The intermediate node Y is necessary, otherwise the average level of X cannot encode the frequency of I_b [19].

For simplicity, we assume that the average level of X determines the axon length,

$$L = \alpha_X \langle X \rangle, \tag{27}$$

where $\langle X \rangle$ is the time average of X. If X is at equilibrium, $\langle X \rangle$ is equal to X. If X is oscillating, $\langle X \rangle$ is the average of X over a period. The biological assumption underlying Eq. (27) is that X positively regulates the length L. Eq. (27) is the simplest way to capture this mathematically. More complicated models may include a differential equation for L [36, 37], where the extension rate or retraction rate depends on X. However, the result is still the existence of a (nonlinear) positive correlation between L and X. Choosing any such nonlinear structure does not change our conclusions; we elected to proceed with Eq. (27) for analytic tractability of our model. Equation (27) together with Eqs. (8) and (24) gives

$$T = \alpha_T \langle X \rangle, \tag{28}$$

where

$$\alpha_T = \alpha_X \left(\frac{2}{\nu_K (1 - \rho_{K,\text{bulk}})} + \frac{2}{\nu_D (1 - \rho_{D,\text{bulk}})} \right). \tag{29}$$

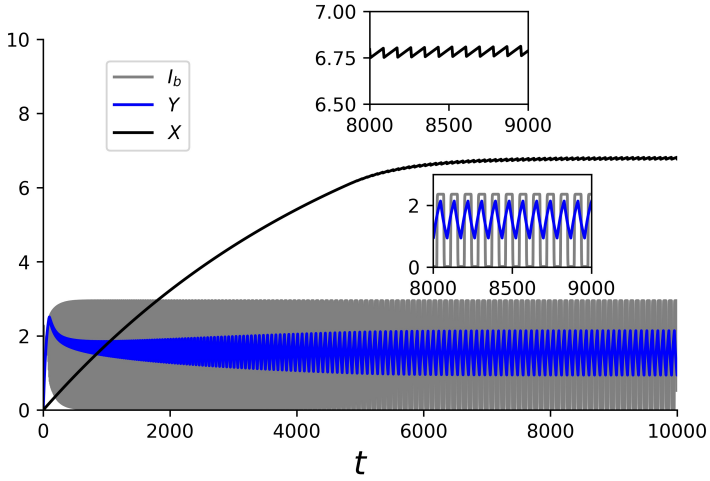

Figure 9: Time evolution of I_b, Y and X in the closed-loop model. The MATLAB solver "ddesd" is used to solve Eqs. (31) and (32) together with Eqs. (1)–(4) simultaneously. The delays at each time step are set according to $\tau_K = \alpha_X X/(\nu_K(1-\rho_{K,\text{bulk}}))$ and $\tau_D = \alpha_X X/(\nu_D(1-\rho_{D,\text{bulk}}))$ and taking advantage of the much slower change in X than I_b and Y so that it approximately constant over an oscillation period. The black curve shows that as the mean value of X equilibrates, so does the axon length. Parameter values are listed in Table 1 and Table 2. All quantities, including X, Y and the four signal concentrations, are initially set to zero.

From Eqs. (27)–(29), we can see that the period is determined by the length through the following relation:

$$T = L\left(\frac{2}{\nu_K(1-\rho_{K,\text{bulk}})} + \frac{2}{\nu_D(1-\rho_{D,\text{bulk}})}\right). \tag{30}$$

T also influences the time evolution of L. This mutual feedback leads to an equilibrium length which we derive in the following.

With the signaling pathway (Eq. (26)), we have the following equations for the time evolution of activated Y and X

$$\frac{\mathrm{d}Y}{\mathrm{d}t} = p_Y(1-\theta(I_b - K_Y)) - d_Y Y, \tag{31}$$

$$\frac{\mathrm{d}X}{\mathrm{d}t} = p_X - (d_X - d_{X,Y}\theta(Y - K_X))X, \tag{32}$$

where θ is the Heaviside function, given by

$$\theta(x) = \begin{cases} 0, & x < 0 \\ 1, & x \geq 0 \end{cases}. \tag{33}$$

The first term in Eq. (31) describes activation of Y that can be inhibited by I_b if I_b is above a threshold K_Y (similar to the inhibition of E_b production by I_b), while the second term describes linear deactivation of Y. p_Y and d_Y are activation and deactivation rate constants. The second term in Eq. (32) ensures that Y promotes X by repressing its deactivation when Y is above another threshold K_X. ($d_{X,Y} < d_X$ for the system to remain bounded.) The first term in this equation, p_X, is the activation rate of X, which is not affected by Y.

At this point, the model forms a closed-loop system, where axon growth is determined by the period of oscillation of I_b and, in turn, the period of the oscillation depends on the axon length. A simulation of the full model is shown in Fig. 9. Initially, the oscillations in I_b (grey curve) are fast and of small amplitude, so that Y (blue) is large. This allows for rapid growth in $\langle X\rangle$ (black curve shows X, with evident rise in mean value). As $\langle X\rangle$, and thus axon length, continues to grow, the oscillation period in I_b increases, resulting in a decline in the mean value of Y. Consequently, $\langle X\rangle$ levels off to an asymptotic value. At this point, there are still small oscillations in X (upper inset), but its mean has equilibrated. Thus, oscillations and axon growth interact to achieve an equilibrium length.

The key element of equilibrated axon length with the close-loop model is increased inhibition of growth with greater oscillation period of I_b. We next show that this is true in general. We first aim at obtaining $\langle X\rangle_\infty$, the value of $\langle X\rangle$ when the means and oscillation amplitudes of I_b, Y and X are at asymptotic levels (i.e., after transients have died out). The lower inset in Fig. 9 indicates that we can ignore the rapid transition of I_b from one level to the other so that it can be approximated by a square wave. We show this approximating square wave together with time evolutions of Y and X in Fig. 10. Note that I_b spends the same amount of time at its maximum and minimum values within a period, which is approximately $\tau_K + \tau_D \equiv D$. During the cycle in Fig. 10A, which starts at t_0, Y evolves as:

$$\frac{\mathrm{d}Y}{\mathrm{d}t} = \begin{cases} -d_Y Y & t_0 \leq t \leq t_0 + D, \\ p_Y - d_Y Y & t_0 + D \leq t \leq t_0 + 2D. \end{cases} \tag{34}$$

Parameter	Definition	Value
p_Y	Basal activation rate of Y	0.0585
d_Y	Basal deactivation rate of Y	0.0195
K_Y	Threshold for I_b to suppress activation of Y	2.25
p_X	Basal activation rate of X	0.0019
d_X	Basal deactivation rate of X	0.0019
$d_{X,Y}$	Reduction in the deactivation rate of X due to Y	0.0018
K_X	Threshold for Y to suppress the deactivation X	1
α_X	Scale factor linking $\langle X \rangle$ to L	1.5

Table 2: Parameter values for the signaling pathway (Eq. (26)).

Y starts each cycle from a maximum value $Y_{\max}$, arrives at $Y_{\min}$ halfway through, and returns to $Y_{\max}$ at the end. By solving Eq. (34), we obtain

$$Y = \begin{cases} Y_{\max} e^{-d_Y (t-t_0)} & t_0 \le t \le t_0 + D, \\ Y_s - (Y_s - Y_{\min}) e^{-d_Y (t-t_0-D)} & t_0 + D \le t \le t_0 + 2D, \end{cases} \tag{35}$$

where $Y_s (= p_Y/d_Y)$ is the equilibrium value of Y in the absence of inhibition by I_b. Imposing continuity at the midpoint of the cycle gives

$$Y_{\min} = Y_s \frac{1}{e^{d_Y D} + 1}, \tag{36}$$

$$Y_{\max} = Y_s \frac{e^{d_Y D}}{e^{d_Y D} + 1}. \tag{37}$$

Let D_Y be the amount of time per oscillation that Y is above K_X, and r_Y be the ratio of this duration to the period (i.e., $r_Y = D_Y/T$). Also define E_Y as the amount of time per oscillation when I_b is below K_X. Thus, $E_Y + D_Y = T$. Under the condition that $Y_{\min} < K_X < Y_{\max}$, we obtain r_Y as

$$r_Y = \frac{1}{2} + \frac{\beta_Y}{T}, \tag{38}$$

where $\beta_Y = \ln((Y_s/K_X) - 1)/d_Y$. We showed in Section (4) that the inhibition due to oscillation becomes stronger as the period T increases. To correctly describe this, we require that $\beta_Y > 0$, which implies $K_X < Y_s/2$. Thus, as an axon grows, T becomes larger and r_Y gets smaller, which means that the growth is less sustained throughout a cycle.

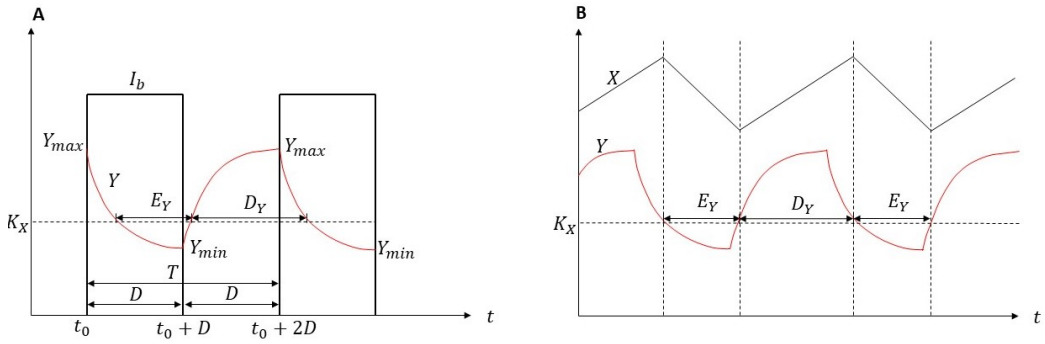

Figure 10: The evolution of I_b, Y and X in the long run. (a) Y declines from $Y_{\max}$ to $Y_{\min}$ when I_b is in its upper level and returns to $Y_{\max}$ again when I_b is in its lower level. D_Y and E_Y are the durations when Y is above and below K_X, respectively. D is the duration when I_b stays in either of its two levels and the period T is $2D$. (b) Evolving on a larger time scale, X increases and decreases linearly during D_Y and E_Y, respectively.

Now we consider $\langle X \rangle$. Note that X evolves as a piecewise linear function, indicated by the upper inset in Fig. 9 and also schematically shown in Fig. 10B. This reflects the fact that X is a slow variable on the time scale of an oscillation period and is related to the production of materials in the cell body. After transient changes in the mean and amplitude of X, the oscillation of X becomes stable and there is no net change in X during each cycle, as shown in Fig. 10B. Therefore, integrating Eq. (32) from some time t_0 over one period T gives us

$$0 = \int_{t_0}^{t_0+T} \frac{\mathrm{d}X}{\mathrm{d}t} \mathrm{d}t = \int_{t_0}^{t_0+T} [p_X - (d_X - d_{X,Y}\theta(Y - K_X))X] \mathrm{d}t. \tag{39}$$

According to the definitions of D_Y and E_Y, Eq. (39) becomes

$$p_X D_Y - (d_X - d_{X,Y}) \int_{t_0}^{t_0+D_Y} X \mathrm{d}t + p_X E_Y - d_X \int_{t_0+D_Y}^{t_0+T} X \mathrm{d}t = 0 \tag{40}$$

Since X evolves linearly during D_Y and E_Y, we have

$$\int_{t_0}^{t_0+D_Y} X\mathrm{d}t = D_Y\langle X\rangle_\infty, \quad \int_{t_0+D_Y}^{t_0+T} X\mathrm{d}t = E_Y\langle X\rangle_\infty, \tag{41}$$

where $\langle X\rangle_\infty$ denotes the equilibrium level of $\langle X\rangle$, achieved at sufficiently large t. Then Eq. (40) becomes

$$[p_X - (d_X - d_{X,Y})\langle X\rangle_\infty]D_Y + (p_X - d_X\langle X\rangle_\infty)E_Y = 0, \tag{42}$$

which yields

$$\langle X\rangle_\infty = \frac{p_X}{d_X - d_{X,Y}r_Y}. \tag{43}$$

We next compare our results to the experiments in [13], where the oscillation period of I_b was changed by partially removing motors from axons. The following closed system determines the oscillation period T and the equilibrium axon length L_∞:

$$\begin{cases} \langle X\rangle_\infty = \frac{p_X}{d_X - d_{X,Y}r_Y}, \\ r_Y = \frac{1}{2} + \frac{\beta_Y}{T}, \\ T = \alpha_T\langle X\rangle_\infty, \\ L_\infty = \alpha_X\langle X\rangle_\infty. \end{cases} \tag{44}$$

We define the rescaled equilibirum length l_∞ by

$$l_\infty \coloneqq \frac{L_\infty}{L_0} = \frac{\alpha_X\langle X\rangle_\infty}{\alpha_X\langle X\rangle_0} = \frac{\langle X\rangle_\infty}{X_0}, \tag{45}$$

where X_0 is the equilibrium value of X when there is no inhibition on the growth, given by

$$X_0 = \frac{p_X}{d_X - d_{X,Y}}. \tag{46}$$

Solving Eq. (44) then gives

$$l_\infty = \frac{cr_d + 2(1 - r_d)}{2 - r_d}, \tag{47}$$

where

$$r_d \equiv \frac{d_{X,Y}}{d_X}, \quad c \equiv \frac{2\beta_Y}{\alpha_T X_0}. \tag{48}$$

Note that c is a function of α_T and α_T is a function of $\rho_{K,\mathrm{bulk}}$ and $\rho_{D,\mathrm{bulk}}$ (Eq. (29)). Thus Eq. (47) relates l_∞ to the bulk densities of motors. To reproduce the experimental data in [13], we consider the limiting case where $l_\infty = c$ (i.e. $r_d \to 1$). For simplicity, we also assume $\nu_K = \nu_D$. In [13], either or both of $\rho_{K,\mathrm{bulk}}$ and $\rho_{D,\mathrm{bulk}}$ were reduced by 40%. Starting with $\rho_{K,\mathrm{bulk}} = \rho_{D,\mathrm{bulk}} = 0.5$, we obtain a 17% increase in l_∞ when either $\rho_{K,\mathrm{bulk}}$ or $\rho_{D,\mathrm{bulk}}$ is reduced to 0.3, and a 40% increase if both are reduced to 0.3. These predictions match the data in [13], which demonstrates that the signaling pathway proposed in the beginning of this section captures experimental observations.

Thus far, we have focused on the equilibrium length when Y oscillates about K_X. If Y is always above K_X the growth is never inhibited and $l_\infty = 1$. Conversely, if Y stays below K_X, the growth is inhibited throughout a cycle and $l_\infty = 1 - r_d$. In summary, we have

$$l_\infty = \begin{cases} 1 & \text{if } Y(t) > K_X \text{ for all } t, \\ \frac{cr_d + 2(1-r_d)}{2-r_d} & \text{if } Y(t) \text{ oscillates and } Y_{\min} < K_X < Y_{\max}, \\ 1 - r_d & \text{if } Y(t) < K_X \text{ for all } t, \end{cases} \tag{49}$$

which describes three equilibrium states: (1) an uninhibited state, (2) a partially inhibited state and (3) and a fully inhibited state. The growth observed experimentally in [20] when the binding affinity between kinesin motors and signal E molecules was reduced corresponds, in our model, to a switch from the second state to the first . The growth observed experimentally in [13] when the motor densities were reduced corresponds, in our model, to an increase in l_∞ due to a change in c. During normal development, an axon would grow freely in the beginning and reach an equilibrium length due to partial inhibition by the oscillation, which is a transition from the first state to the second. The third state cannot be reached in this case and it may correspond to abnormal physiological conditions. In the next section, we will see that changes in some parameters of the delayed feedback model can drive l_∞ to the third case.

6 The model predicts steps in axon length

In this section we use numerical continuation of the full closed-loop model to analyze the dependence of the equilibrium axon length on model parameters. To increase the biological fidelity of our model, we replace the Heaviside functions used in production and degradation terms for mathematical convenience previously with Hill functions. Thus, the dynamics of X and Y are now described by

$$\frac{\mathrm{d}Y}{\mathrm{d}t} = p_Y(1 - H\left(I_b, K_Y, n_Y\right)) - d_Y Y, \tag{50}$$

$$\frac{\mathrm{d}X}{\mathrm{d}t} = p_X - (d_X - d_{X,Y} H\left(Y, K_X, n_X\right))X. \tag{51}$$

where $H\left(\cdot,\cdot,\cdot\right)$ is defined in Eq. (6) with $n_X = n_Y = 5$.

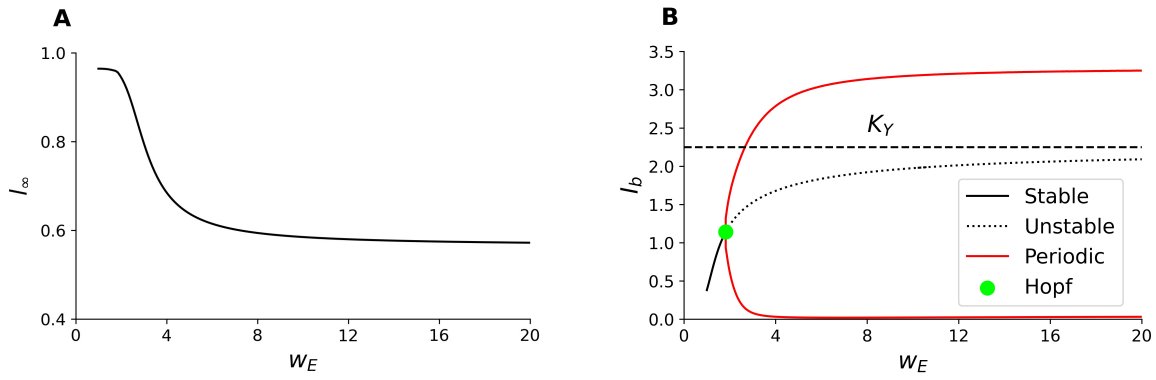

Figure 11: The variation of equilibrium axon length with variation in w_E, the number of E molecules carried by a single kinesin motor. (A) The equilibrium length exhibits a step down as w_E is increased. (B) The bifurcation diagram has a single Hopf bifurcation. The threshold for inhibition of Y is superimposed as a dashed line.

We begin by examining the effects of varying w_E, the parameter describing the average number of E molecules carried by a single kinesin motor. For small values of the parameter the equilibrium length is large. As w_E is increased, l_∞ changes little until there is a sharp drop to a lower value (Fig. 11A). This lower value is maintained for the remainder of the range of w_E values examined. Thus, there is a single step down in the equilibrium length as w_E is increased. The reason for this step-like behavior is apparent from the I_b bifurcation diagram (Fig. 11B). Once w_E reaches a value large enough that the peak of the oscillation in I_b exceeds the threshold value K_Y, the signaling molecule Y will be subject to inhibition by I_b (Fig. 11B). Thus, the curves in Fig. 11 reflect a switch from a free-growth state to an inhibited state. Similar behaviors occur when w_I or p_I are varied.

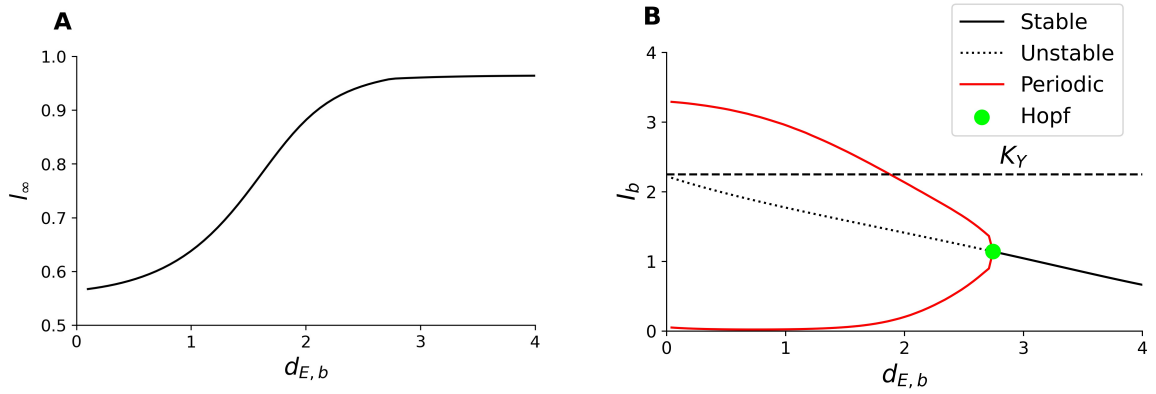

Figure 12: The variation of equilibrium axon length with variation in the degradation parameter $d_{E,b}$. (A) The equilibrium length exhibits a step up as $d_{E,b}$ is increased. (B) The bifurcation diagram in I_b has a single Hopf bifurcation. The threshold for inhibition of Y is superimposed as a dashed line.

We next examine the effects of varying the degradation parameter $d_{E,b}$. For small values of this parameter the equilibrium length is small. As in the previous case, there is a step-like behavior as $d_{E,b}$ is increased, but this time there is an upward step (Fig. 12A). This upward step occurs when the peak value of I_b during an oscillation falls below K_Y, which removes inhibition of Y. This results in an increase in the equilibrium $\langle X \rangle$ and thus an increase in the equilibrium axon length. The equilibrium axon length exhibits similar upward step behaviors when $d_{I,b}$ or $d_{I,t}$ are increased.

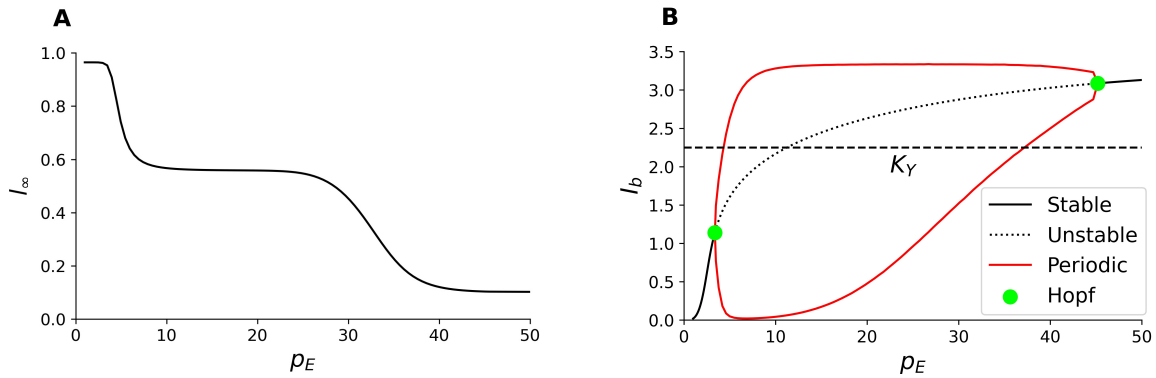

Figure 13: The variation of equilibrium axon length with variation in the E production parameter p_E. (A) The equilibrium length exhibits two steps down as p_E is increased. (B) The bifurcation diagram in I_b has two Hopf bifurcations. The threshold for inhibition of Y is superimposed as a dashed line.

Unlike the cases above, there is a two-step decrease in l_∞ as p_E, the basal production rate of E at the body, is increased (Fig. 13A). The first step down occurs for p_E values just past the initiation of oscillations in I_b. That is, just beyond the left Hopf bifurcation point in the I_b bifurcation diagram (Fig. 13B). The rapid increase in the amplitude of the oscillation that occurs after the bifurcation results in the peak I_b values moving past K_Y, inhibiting Y and reducing the equilibrium axon length. At larger values of p_E a second Hopf bifurcation occurs. As this bifurcation is approached, the peak I_b value is almost unchanged, but the minimum value during the oscillation increases, so that at some point $I_b > K_Y$ throughout the entire oscillation cycle. This case of maximum inhibition of Y by I_b results in a second downward step in the equilibrium axon length and corresponds to the third case in Eq. (49). Biologically, over-production of the signal E molecules leads to a high level of I and prevents the system from oscillating. There is a similar two-step change in l_∞ when $d_{E,t}$ is increased, except that l_∞ increases twice instead of falling twice.

All cases discussed thus far exhibit monotonic increases or decreases of l_∞ when the bifurcation parameter is increased. If we look instead at the effects of changes in the bulk densities of motors the situation is different. Figure 14A shows that l_∞ is initially unaffected by an increase in $\rho_{K,\text{bulk}}$, but then steps down to a lower value. However, once $\rho_{K,\text{bulk}}$ is sufficiently large, there is a step back to the original equilibrium axon length. This result can be explained by an analysis of the I_b bifurcation diagram (Figure 14B), which has two Hopf bifurcations that initiate and terminate the oscillations. For a range of values of $\rho_{K,\text{bulk}}$ between, the peak I_b value of the oscillations is above K_Y so Y is inhibited. Outside of this range Y is not inhibited, so l_∞ takes on its maximum value. Biologically, as $\rho_{K,\text{bulk}}$ increases, the kinesin motors get crowded within an axon. This prevents them from transporting the signal E effectively, which in turn leads to cessation of the oscillation and removal of inhibition from the axon growth mechanism. Similar behavior occurs if $\rho_{D,\text{bulk}}$ is varied.

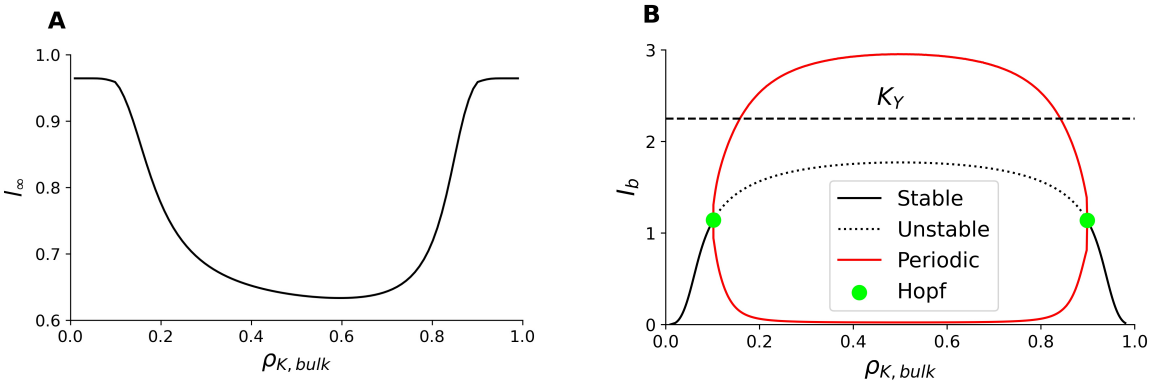

Figure 14: The variation of equilibrium axon length with variation in the kinesin bulk density constant $\rho_{K,\text{bulk}}$. (A) The equilibrium length exhibits a non-monotonic behavior as the bulk density is increased. (B) The bifurcation diagram has two Hopf bifurcations. The threshold for inhibition of Y is superimposed as a dashed line.

7 Discussion

In this article, we developed a multi-scale model of a mechanism for axon length regulation proposed by Rishal et al [13]. Our model extends earlier models [18, 19] by using a TASEP approach to characterize motor dynamics. This enabled us to form a direct link between molecular motor dynamics, signaling delays, and axon length. We further derived a closed system by introducing a gene signaling pathway that maps the oscillation period to the strength of

inhibition for axon growth. This closed-loop model captures the results of two experimental manipulations [13, 20] and yields expressions for equilibrium axon length that has three distinct equilibrium states: (1) a free-growth state, (2) a partially-inhibited state, and (3) a fully inhibited state. Changes in system parameters induce transitions from one state to another. That is, our model links microscopic changes in motor density in an axon to the macroscopic property of axonal length.

One important prediction of our model is that increasing motor density to a sufficiently high value results in axonal growth (Fig. 14). This result manifests from the assumption that the signal oscillation drives inhibition. As far as we know, experimental studies have not investigated such behavior. Such investigation could validate our model and provide circumstantial evidence for inhibition being driven by signal oscillations.

Throughout the paper, we assume that the hopping rates of kinesin and dynein motors are the same. However, data indicate that they can be different [38]. In the current delayed feedback model (Eqs. (1)–(4)), the currents (J_K and J_D) and the delays (τ_K and τ_D) depend on the hopping rates. If $\nu_K > \nu_D$, J_K and τ_K will be more sensitive to a change in $\rho_{K,\text{bulk}}$ than J_D and τ_D to the same change in $\rho_{D,\text{bulk}}$. But this does not qualitatively alter our model results.

To see this point more clearly, consider the equilibrium length l_∞, which is given by Eq. (49). For simplicity, let $r_d \to 1$, so that $l_\infty = c$. By the definitions of c (Eq. (48)) and α_T (Eq. (29)), we get

$$l_\infty \sim \frac{1}{\frac{1}{\nu_K(1-\rho_{K,\text{bulk}})} + \frac{1}{\nu_D(1-\rho_{D,\text{bulk}})}}. \tag{52}$$

From this relation, we can see that l_∞ changes faster with $\rho_{K,\text{bulk}}$ if ν_K is larger. However, l_∞ still decreases with $\rho_{K,\text{bulk}}$ or $\rho_{D,\text{bulk}}$ and this result matches the experimental observation in [13]. Additionally, J_K appears in a product with w_E in the delayed feedback model (Eqs. (1)–(4)) and they thus play the same role mathematically. Our bifurcation analysis of w_E shows that it only affects the oscillation amplitude, not the frequency (Fig. 7). Therefore, an increase in J_K due to larger ν_K will not affect the oscillation frequency. Furthermore, the bifurcation diagram with respect to $\rho_{K,\text{bulk}}$ will not change qualitatively for a larger ν_K, although the Hopf bifurcation points may change their locations. Thus, our prediction regarding equilibrium length (Fig. 14) remains the same. The above discussion also applies to ν_D.

To model the transportation of motors, we used two uncoupled TASEPs in opposite directions. In reality, kinesin and dynein motors share the same tracks and their steric interactions reduce the currents of both motors and prolong the delays to traverse the axon. Indeed, a recent study shows that co-existence of two types of motors hinder their motions [38]. However, the current-density and delay-density relations remain qualitatively the same in this case. That is, for small densities, the current increases as a function of density until a critical value is reached, beyond which the current decreases with motor density to zero. Moreover, delay times to traverse the axon increases with increasing motor density. Thus, the conclusions in this paper do not change.

Another complexity our model fails to explicitly capture is that some cargoes are attached to both motors simultaneously and their motion is bidirectional [39, 40]. It is possible that our hypothesized chemical signals' dynamics undergo bidirectional motion. In spite of this, we expect the average excitatory signal current to be in the anterograde direction and the average inhibitory signal current to be in the retrograde direction. Thus, we expect the qualitative behavior of our model in this case to be similar to the model we analyzed in this paper, albeit perhaps with smaller motor currents and longer delays.

There are a number of issues we hope to explore in future work. First, we hope to capture finer details of motor transport with a mathematical model. For example, motors detach from microtubules, diffuse in cytosol, and reattach to the microtubules during cargo transport. To model these phenomena, a two-lane lattice system can be used where one lane describes the active motor movement along microtubules and the other lane describes their passive diffusion [27, 41–44]. The attachment and detachment can be modeled as a switch between the two lanes. More generally, we can frame transitions in the states of molecular motors and the corresponding dynamics as a piecewise deterministic Markov process [24, 45–47], wherein a Markov process governs transitions between microscopic states and the dynamics in each state are deterministic. Indeed, motor-driven cargo exhibits ballistic anterograde or retrograde motion interspersed with periods of long pauses [26]. Incorporating such details will allow us to better characterize the effect of noise at the motor level on the full system.

Second, we hope to incorporate intrinsic noise in gene activation states into the model. Our signaling pathway implicitly assumes a large copy number for the number of gene states and therefore allows us to use kinetic equations to describe protein dynamics in response to the oscillating retrograde signal. If copy numbers are low, a master equation needs to be constructed to describe the dynamics and can be useful to quantitate intrinsic noise. Though this has been done previously [19, 48], our formulation is more general in that we make no attempt to specify cellular processes affected by oscillatory signals.

Finally, we note that an alternative axonal length-sensing mechanism has been proposed [49]. There, Roossien et al. tracked the movement of docked mitochondria in order to establish that the physical mechanism of growth cone advance in Drosophila is similar to vertebrate neurons. That is, the bulk forward translocation of microtubules along the axon underlies the advance of the growth cone C-domain. They also compared the length of axons grown on two different substrates, either poly-ornithine or Drosophila ExtraCellular Matrix (DECM). They found that axons grown on the faster substrate DECM ended up being longer than the other substrate. The authors suggested that if a length sensor were the sole regulator of the cessation of elongation, then neurons grown on poly-ornithine would be expected

to sustain elongation for a longer time than neurons grown on DECM so that they end up having similar lengths. Since this was not observed, it suggests that there may be some internal clock that is independent of axonal length and terminates elongation after a set period of growth.

Appendix A: Derivation of Eq. (14)

Here we show how to obtain the relation

$$r_i = \frac{1}{\nu_K(1-\rho_{K,i})} \tag{A.1}$$

from

$$r_i = \sum_{n=1}^{\infty} n\mathrm{d}t(1-\rho_{K,i})\nu_K\mathrm{d}t(1-(1-\rho_{K,i})\nu_K\mathrm{d}t)^{n-1}. \tag{A.2}$$

Let $A = (1-\rho_{K,i})\nu_K\mathrm{d}t$, then we have

$$r_i = A\mathrm{d}t\sum_{n=1}^{\infty} n(1-A)^{n-1} = A\mathrm{d}tS, \tag{A.3}$$

where

$$S = \sum_{n=1}^{\infty} n(1-A)^{n-1} = 1\cdot(1-A)^0 + 2\cdot(1-A)^1 + \cdots. \tag{A.4}$$

Multiplying both sides of this equation by $1-A$ gives

$$(1-A)S = 1\cdot(1-A)^1 + 2\cdot(1-A)^2 + \cdots. \tag{A.5}$$

Substracting Eq. (A.5) from Eq. (A.4) gives

$$AS = (1-A)^0 + (1-A)^1 + \cdots = \frac{1}{A}. \tag{A.6}$$

Therefore we have

$$S = \frac{1}{A^2} \tag{A.7}$$

and

$$r_i = A\mathrm{d}t\cdot\frac{1}{A^2} = \frac{\mathrm{d}t}{A} = \frac{1}{\nu_K(1-\rho_{K,i})}. \tag{A.8}$$

Appendix B: Nondimensionalization of the delayed feedback model

Hew we show how Eqs. (20)–(25) are derived by properly choosing characteristic scales for model parameters. We first select the following rescaled parameters

$$\tilde{\tau}_K = \frac{\tau_K}{t^*}, \quad \tilde{l} = \frac{l}{l^*}, \quad \tilde{a} = \frac{a}{l^*}, \quad \tilde{\nu}_K = \frac{\nu_K}{\nu^*}, \tag{B.1}$$

where we use tildes for the dimensionless parameters and stars for their characteristic scales. Thus, Eq. (16) becomes

$$\tilde{\tau}_K = \frac{\tilde{l}}{\tilde{a}\tilde{\nu}_K(1-\rho_{K,\mathrm{bulk}})t^*v^*}. \tag{B.2}$$

The characteristic time scale t^* for motion along the microtubules will be inversely proportional to the hopping rate, so we set $t^* = 1/v^*$. Then,

$$\tilde{\tau}_K = \frac{\tilde{l}}{\tilde{a}\tilde{\nu}_K(1-\rho_{K,\mathrm{bulk}})}. \tag{B.3}$$

For dynein motors, we have a similar relation

$$\tilde{\tau}_D = \frac{\tilde{l}}{\tilde{a}\tilde{\nu}_D(1-\rho_{D,\mathrm{bulk}})}. \tag{B.4}$$

To nondimensionalize the equations (Eqs. (1)–(4)), we use the rescaling

$$\tilde{E}_b = \frac{E_b}{E^*}, \quad \tilde{E}_t = \frac{E_t}{E^*r_V}, \quad \tilde{I}_b = \frac{r_V I_b}{E^*}, \quad \tilde{I}_t = \frac{I_t}{E^*}, \tag{B.5}$$

$$\tilde{p}_E = \frac{t^*}{E^*}p_E, \quad \tilde{p}_I = \frac{t^*}{E^*}p_I, \quad \tilde{K}_E = \frac{K_E}{E^*r_V}, \quad \tilde{K}_I = \frac{r_V K_I}{E^*}, \tag{B.6}$$

$$\tilde{d}_{E,b} = t^*d_{E,b}, \quad \tilde{d}_{E,t} = t^*d_{E,t}, \quad \tilde{d}_{I,b} = t^*d_{I,b}, \quad \tilde{d}_{I,t} = t^*d_{I,t}. \tag{B.7}$$

Then we have

$$\frac{\mathrm{d}\tilde{E}_b}{\mathrm{d}t} = \tilde{p}_{E,b} - \tilde{d}_{E,b}\tilde{E}_b(t) - \frac{w_E}{\tilde{a}}\tilde{J}_K\tilde{E}_b(t), \tag{B.8}$$

$$\frac{\mathrm{d}\tilde{E}_t}{\mathrm{d}t} = -\tilde{d}_{E,t}\tilde{E}_t(t) + \frac{w_E}{\tilde{a}}\tilde{J}_K\tilde{E}_b(t-\tau_K), \tag{B.9}$$

$$\frac{\mathrm{d}\tilde{I}_b}{\mathrm{d}t} = -\tilde{d}_{\tilde{I},b}\tilde{I}_b(t) + \frac{w_I}{\tilde{a}}\tilde{J}_D\tilde{I}_t(t-\tau_D), \tag{B.10}$$

$$\frac{\mathrm{d}\tilde{I}_t}{\mathrm{d}t} = \tilde{p}_{\tilde{I},t} - \tilde{d}_{I,t}I_t(t) - \frac{w_E}{\tilde{a}}\tilde{J}_D\tilde{I}_t(t), \tag{B.11}$$

where

$$\tilde{p}_{E,b} = \tilde{p}_E\frac{\tilde{E}_b^{n_E}}{\tilde{E}_b^{n_E} + \tilde{K}_E^{n_E}}, \quad \tilde{p}_{I,t} = \tilde{p}_I\frac{\tilde{I}_t^{n_I}}{\tilde{I}_t^{n_I} + \tilde{K}_I^{n_I}} \tag{B.12}$$

$$\tilde{J}_K = \tilde{a}\tilde{\nu}_K\rho_{K,\mathrm{bulk}}(1-\rho_{K,\mathrm{bulk}}), \quad \tilde{J}_D = \tilde{a}\tilde{\nu}_D\rho_{D,\mathrm{bulk}}(1-\rho_{D,\mathrm{bulk}}). \tag{B.13}$$

For convenience, we still use $\tilde{\nu}_K$ and $\tilde{\nu}_D$ for $\tilde{a}\tilde{\nu}_K$ and $\tilde{a}\tilde{\nu}_D$, and $\tilde{w}_E$ and $\tilde{w}_I$ for $\tilde{w}_E/\tilde{a}$ and $\tilde{w}_I/\tilde{a}$. Only the dimensionless equations will be used in the following, so we drop all the tildes to obtain

$$\frac{\mathrm{d}E_b(t)}{\mathrm{d}t} = p_{E,b}(t) - d_{E,b}E_b(t) - w_E J_K E_b(t), \tag{B.14}$$

$$\frac{\mathrm{d}E_t(t)}{\mathrm{d}t} = -d_{E,t}E_t(t) + w_E J_K E_b(t-\tau_K), \tag{B.15}$$

$$\frac{\mathrm{d}I_b(t)}{\mathrm{d}t} = -d_{I,b}I_b(t) + w_I J_D I_t(t-\tau_D), \tag{B.16}$$

$$\frac{\mathrm{d}I_t(t)}{\mathrm{d}t} = p_{I,t}(t) - d_{I,t}I_t(t) - w_I J_D I_t(t), \tag{B.17}$$

with the relations for the dimensionless delays and currents

$$\tau_K = \frac{l}{\nu_K(1-\rho_{K,\mathrm{bulk}})}, \quad \tau_D = \frac{l}{\nu_D(1-\rho_{D,\mathrm{bulk}})} \tag{B.18}$$

$$J_K = \nu_K\rho_{K,\mathrm{bulk}}(1-\rho_{K,\mathrm{bulk}}), \quad J_D = \nu_D\rho_{D,\mathrm{bulk}}(1-\rho_{D,\mathrm{bulk}}). \tag{B.19}$$

Author Contributions

RB and BK designed the research. FB, RB, and BK developed the analysis. FB ran all numerical simulations. FB, RB, and BK wrote and edited the paper.

Competing Interests

The authors declare that no competing interests exist.

Acknowledgement

We thank Frederic Folz, Isabella Graf, and Cécile Appert-Rolland for helpful discussions.

References

[1] Eric R. Kandel, James H. Schwartz, Thomas M. Jessell, Steven A. Siegelbaum, and A. J. Hudspeth, editors. Principles of neural science. McGraw-Hill, 5 edition, 2013.

[2] Christin A. Albus, Ida Rishal, and Mike Fainzilber. Cell length sensing for neuronal growth control. Trends in Cell Biology, 23(7):305–310, July 2013.

[3] Douglas H. Smith. Stretch growth of integrated axon tracts: Extremes and exploitations. Progress in Neurobiology, 89(3):231–239, November 2009.

[4] Pierre Recho, Antoine Jerusalem, and Alain Goriely. Growth, collapse, and stalling in a mechanical model for neurite motility. Phys. Rev. E, 93:032410, March 2016.

[5] Bruce Alberts, Alexander Johnson, Julian Lewis, David Morgan, Martin Raff, Keith Roberts, Peter Walter, John Wilson, and Tim Hunt. Molecular biology of the cell. WW Norton & Company, 2017.

[6] Samara L. Reck-Peterson, William B. Redwine, Ronald D. Vale, and Andrew P. Carter. The cytoplasmic dynein transport machinery and its many cargoes. Nature Reviews Molecular Cell Biology, 19(6):382–398, June 2018.

[7] C. Appert-Rolland, M. Ebbinghaus, and L. Santen. Intracellular transport driven by cytoskeletal motors: General mechanisms and defects. Physics Reports, 593:1 – 59, September 2015. Intracellular transport driven by cytoskeletal motors: General mechanisms and defects.

[8] Irene Dalla Costa, Courtney N. Buchanan, Matthew D. Zdradzinski, Pabitra K. Sahoo, Terika P. Smith, Elizabeth Thames, Amar N. Kar, and Jeffery L. Twiss. The functional organization of axonal mrna transport and translation. Nature Reviews Neuroscience, 22(2):77–91, February 2021.

[9] Maria-Veronica Ciocanel, Bjorn Sandstede, Samantha P Jeschonek, and Kimberly L Mowry. Modeling microtubule-based transport and anchoring of mrna. SIAM journal on applied dynamical systems, 17(4):2855–2881, 2018.

[10] Bhargav R Karamched and Paul C Bressloff. Effects of cell geometry on reversible vesicular transport. Journal of Physics A: Mathematical and Theoretical, 50(5):055601, 2017.

[11] Paul C Bressloff and Bin Xu. Stochastic active-transport model of cell polarization. SIAM Journal on Applied Mathematics, 75(2):652–678, 2015.

[12] Abhimanyu Sharma and Michael Vershinin. Length dependence of the rigidity of microtubules in small networks. Biochemical and Biophysical Research Communications, 529(2):303–305, 2020.

[13] Ida Rishal, Naaman Kam, Rotem Ben-Tov Perry, Vera Shinder, Elizabeth M. Fisher, Giampietro Schiavo, and Mike Fainzilber. A motor-driven mechanism for cell-length sensing. Cell Reports, 1(6):608 – 616, June 2012.

[14] Ida Rishal and Mike Fainzilber. Cell size sensing—a one-dimensional solution for a three-dimensional problem? BMC biology, 17(1):36, April 2019.

[15] Ida Rishal and Mike Fainzilber. Axon–soma communication in neuronal injury. Nature Reviews Neuroscience, 15(1):32–42, December 2014.

[16] Filipe Tostevin, Wiet de Ronde, and Pieter Rein ten Wolde. Reliability of frequency and amplitude decoding in gene regulation. Phys. Rev. Lett., 108:108104, March 2012.

[17] Gabriele Micali, Gerardo Aquino, David M. Richards, and Robert G. Endres. Accurate encoding and decoding by single cells: Amplitude versus frequency modulation. PLOS Computational Biology, 11(6):e1004222, June 2015.

[18] Bhargav R. Karamched and Paul C. Bressloff. Delayed feedback model of axonal length sensing. Biophysical Journal, 108(9):2408 – 2419, May 2015.

[19] Frederic Folz, Lukas Wettmann, Giovanna Morigi, and Karsten Kruse. Sound of an axon's growth. Physical Review E, 99:050401, May 2019.

[20] Rotem B. Perry, Ida Rishal, Ella Doron-Mandel, Ashley L. Kalinski, Katalin F. Medzihradszky, Marco Terenzio, Stefanie Alber, Sandip Koley, Albina Lin, Meir Rozenbaum, Dmitry Yudin, Pabitra K. Sahoo, Cynthia Gomes, Vera Shinder, Wasim Geraisy, Eric A. Huebner, Clifford J. Woolf, Avraham Yaron, Alma L. Burlingame, Jeffery L. Twiss, and Mike Fainzilber. Nucleolin-mediated Rna localization regulates neuron growth and cycling cell size. Cell Reports, 16(6):1664 – 1676, August 2016.

[21] MATLAB. Version R2021a Update 3 (9.10.01684407). The MathWorks Inc., Natick, Massachusetts, United States, 2021.

[22] T Chou, K Mallick, and R K P Zia. Non-equilibrium statistical mechanics: from a paradigmatic model to biological transport. Reports on Progress in Physics, 74(11):116601, oct 2011.

[23] Paul C. Bressloff and Jay M. Newby. Stochastic models of intracellular transport. Reviews of Modern Physics, 85:135–196, Jan 2013.

[24] Paul C. Bressloff. Diffusion in cells with stochastically gated gap junctions. SIAM Journal on Applied Mathematics, 76(4):1658–1682, August 2016.

[25] R A Blythe and M R Evans. Nonequilibrium steady states of matrix-product form: a solver's guide. Journal of Physics A: Mathematical and Theoretical, 40(46):R333–R441, oct 2007.

[26] Celine I. Maeder, Adriana San-Miguel, Emily Ye Wu, Hang Lu, and Kang Shen. In vivo neuron-wide analysis of synaptic vesicle precursor trafficking. Traffic, 15(3):273–291, December 2014.

[27] Isabella R. Graf and Erwin Frey. Generic transport mechanisms for molecular traffic in cellular protrusions. Physical Review Letters, 118:128101, March 2017.

[28] J. Messelink, R. Rens, M. Vahabi, F. C. MacKintosh, and A. Sharma. On-site residence time in a driven diffusive system: Violation and recovery of a mean-field description. Phys. Rev. E, 93:012119, January 2016.

[29] Bernard Derrida, Eytan Domany, and David Mukamel. An exact solution of a one-dimensional asymmetric exclusion model with open boundaries. Journal of Statistical Physics, 69(3-4):667–687, November 1992.

[30] B Derrida, M R Evans, V Hakim, and V Pasquier. Exact solution of a 1d asymmetric exclusion model using a matrix formulation. Journal of Physics A: Mathematical and General, 26(7):1493–1517, April 1993.

[31] G. Schütz and E. Domany. Phase transitions in an exactly soluble one-dimensional exclusion process. Journal of statistical physics, 72(1-2):277–296, July 1993.

[32] Koen Engelborghs, Tatyana Luzyanina, and Giovanni Samaey. Dde-biftool v. 2.00: a matlab package for bifurcation analysis of delay differential equations, 2001.

[33] Zhigang He and Yishi Jin. Intrinsic control of axon regeneration. Neuron, 90(3):437–451, May 2016.

[34] Zofia M. Lasiecka and Bettina Winckler. Mechanisms of polarized membrane trafficking in neurons — focusing in on endosomes. Molecular and Cellular Neuroscience, 48(4):278–287, December 2011. Membrane Trafficking and Cytoskeletal Dynamics in Neuronal Function.

[35] Christine E. Holt and Erin M. Schuman. The central dogma decentralized: New perspectives on rna function and local translation in neurons. Neuron, 80(3):648–657, October 2013.

[36] Michinori Toriyama, Yuichi Sakumura, Tadayuki Shimada, Shin Ishii, and Naoyuki Inagaki. A diffusion-based neurite length-sensing mechanism involved in neuronal symmetry breaking. Molecular Systems Biology, 6(1):394, 2010.

[37] Marc Fivaz, Samuel Bandara, Takanari Inoue, and Tobias Meyer. Robust neuronal symmetry breaking by ras-triggered local positive feedback. Current Biology, 18(1):44–50, 2008.

[38] Patrick Wilke, Emanuel Reithmann, and Erwin Frey. Two-species active transport along cylindrical biofilaments is limited by emergent topological hindrance. Phys. Rev. X, 8:031063, September 2018.

[39] Melanie J. I. Müller, Stefan Klumpp, and Reinhard Lipowsky. Tug-of-war as a cooperative mechanism forbidirectional cargo transport by molecular motors. Proceedings of the National Academy of Sciences, 105(12):4609–4614, 2007.

[40] Sudipto Muhuri, Lenin Shagolsem, and Madan Rao. Bidirectional transport in a multispecies totally asymmetric exclusion-process model. Phys. Rev. E, 84:031921, Sep 2011.

[41] Mareike Bojer, Isabella R. Graf, and Erwin Frey. Self-organized system-size oscillation of a stochastic lattice-gas model. Physical Review E, 98:012410, July 2018.

[42] Vandana Yadav, Rajesh Singh, and Sutapa Mukherji. Phase-plane analysis of driven multi-lane exclusion models. Journal of Statistical Mechanics: Theory and Experiment, 2012(4):P04004, April 2012.

[43] Melanie J. Müller, Stefan Klumpp, and Reinhard Lipowsky. Molecular motor traffic in a half-open tube. Journal of Physics: Condensed Matter, 17(47):S3839–S3850, November 2005.

[44] M R Evans, Y Kafri, K E P Sugden, and J Tailleur. Phase diagrams of two-lane driven diffusive systems. Journal of Statistical Mechanics: Theory and Experiment, 2011(06):P06009, June 2011.

[45] P. C. Bressloff and J. M. Newby. Directed intermittent search for hidden targets. New Journal of Physics, 11(2):023033, February 2009.

[46] Paul C. Bressloff and Jay M. Newby. Path integrals and large deviations in stochastic hybrid systems. Phys. Rev. E, 89:042701, April 2014.

[47] Paul C Bressloff and Sean D Lawley. Moment equations for a piecewise deterministic PDE. Journal of Physics A: Mathematical and Theoretical, 48(10):105001, February 2015.

[48] Paul C. Bressloff and Bhargav R. Karamched. A frequency-dependent decoding mechanism for axonal length sensing. Frontiers in Cellular Neuroscience, 9:281, July 2015.

[49] Douglas H. Roossien, Phillip Lamoureux, David Van Vactor, and Kyle E. Miller. Drosophila growth cones advance by forward translocation of the neuronal cytoskeletal meshwork in vivo. PLOS ONE, 8(11):e80136, November 2013.